Matrix lumican endocytosed by immune cells controls receptor ligand trafficking to promote TLR4 and restrict TLR9 in sepsis

George Maiti[a], Jihane Frikeche[b], Carly Yuen-Man Lam[a], Asim Biswas[a], Vishal Shinde[a], Marie Samanovic[c], Jonathan C. Kagan[d], Mark J. Mulligan[c], and Shukti Chakravarti[a,e,1]

[a]Department of Ophthalmology, New York University Grossman School of Medicine, New York, NY 10016; [b]Division of Preclinical Pharmacology and Safety, Sangamo Therapeutics, Valbonne 06560, France; [c]Langone Vaccine Center, New York University, New York, NY 10016; [d]Harvard Medical School and Division of Gastroenterology, Boston Children's Hospital, Boston, MA 02115; and [e]Department of Pathology, New York University Grossman School of Medicine, New York, NY 10016

Edited by Lawrence Steinman, Stanford University School of Medicine, Stanford, CA, and approved May 24, 2021 (received for review January 17, 2021)

Infections and inflammation are profoundly influenced by the extracellular matrix (ECM), but their molecular underpinnings are ill defined. Here, we demonstrate that lumican, an ECM protein normally associated with collagens, is elevated in sepsis patients' blood, while lumican-null mice resolve polymicrobial sepsis poorly, with reduced bacterial clearance and greater body weight loss. Secreted by activated fibroblasts, lumican promotes Toll-like receptor (TLR) 4 response to bacterial lipopolysaccharides (LPS) but restricts nucleic acid–specific TLR9 in macrophages and dendritic cells. The underlying mechanism involves lumican attachment to the common TLR coreceptor CD14 and caveolin 1 (Cav1) in lipid rafts on immune cell surfaces via two epitopes, which may be cryptic in collagen-associated lumican. The Cav1 binding epitope alone is sufficient for cell surface enrichment of Cav1, while both are required for lumican to increase cell surface TLR4, CD14, and proinflammatory cytokines in response to LPS. Endocytosed lumican colocalizes with TLR4 and LPS and promotes endosomal induction of type I interferons. Lumican-null macrophages show elevated TLR9 in signal-permissive endolysosomes and increased response, while wild types show lumican colocalization with CpG DNA but not TLR9, consistent with a ligand sequestering, restrictive role for lumican in TLR9 signaling. In vitro, lumican competes with CD14 to bind CpG DNA; biglycan, a lumican paralog, also binds CpG DNA and suppresses TLR9 response. Thus, lumican and other ECM proteins, synthesized de novo or released from collagen association during ECM remodeling, may be internalized by immune cells to regulate their transcriptional programs and effector responses that may be harnessed in future therapeutics.

lumican | macrophage | TLR | sepsis | inflammation

The extracellular matrix (ECM) maintains homeostatic tissue integrity and an optimal microenvironment for cells (1–3). Components of the ECM released through enzymatic degradation during remodeling or secreted by inflammation-activated fibroblasts are able to interact with soluble factors and cell surface receptors to influence a range of cellular functions (4). These ECM–cell interactions are the foundations for repair and their dysregulations the basis of chronic inflammatory diseases. Sepsis is a global life-threatening inflammatory disease in which inflammation and multiple organ dysfunctions are caused by underlying infection (5). It affects 48.9 million people worldwide, but the role of the ECM in sepsis is unknown. Our human and mouse studies in sepsis uncover a role for a secreted ECM proteoglycan, called lumican, in Toll-like receptor (TLR)–mediated innate immunity and inflammation. Lumican is a member of the leucine-rich repeat (LRR) superfamily (6) of more than 350 proteins, which includes the pathogen recognition TLRs (7). Lumican (*LUM*) and its paralogs, biglycan (*BGN*) and decorin (*DCN*), comprise a subgroup of 16 secreted ECM proteins that were historically known as the small leucine-rich repeat proteoglycans (SLRPs), with their relationship to the LRR superfamily not appreciated early on (8, 9). Many SLRPs colocalize and associate with fibrillar collagens in ECMs of mesenchymal origin and considered structural ECM proteins and proteoglycans. However, they are not all equally present in all tissues or in all developmental stages and consequently have shared and unique functions in different tissues (10). Lumican, biglycan, and decorin maintain collagen fibril structure, tissue integrity, and hydration in different connective tissues (11). Corroboratively, mice systemically lacking *Lum* (12), *Bgn* (13), or *Dcn* (14, 15) have structural collagen defects, corneal opacity, and skin, tendon, or bone fragility.

Multiple studies noted changes in SLRP levels in inflammatory diseases and their mouse models (16–19). We realized that, as LRR superfamily members, SLRPs may share functional similarities with TLRs, prompting us to begin investigating Lum functions in infections and inflammation (20). Thus, we found that $Lum^{-/-}$ mice were impaired in bacterial clearance, showing increased mortality and morbidity in *Pseudomonas* infections of the lungs and cornea (21, 22). While Bgn and Dcn were also reported to promote TLR2 and TLR4 responses at the cell surface (23, 24), molecular mechanisms by which they actually regulate intracellular events in TLR signals remain unclear. Here, we identify paracrine regulation of TLR4 and endosomal TLR9 signals by Lum and Bgn, involving shared and unique interactions with immune cell surface proteins. These interactions involve epitopes

Significance

Sepsis is a life-threatening inflammatory disease of dysregulated innate immune cells. Extracellular matrix (ECM) interactions with immune cells are important in this context and require deeper insights. We show that immune cells ingest lumican, a ubiquitous ECM protein produced by fibroblasts, to heighten their response to bacteria but restrict their response to viral or degraded self-DNA released from dead cells. Sepsis patients have elevated circulating lumican, and mice lacking lumican show poor bacterial clearance and resolution of sepsis but elevated response to DNA. Lumican may play a dual protective role in barrier ECM tissues, one of promoting bacterial defense and another of limiting antiviral and autoimmune inflammatory responses.

Author contributions: G.M. and S.C. designed research; G.M., J.F., C.Y.-M.L., A.B., and V.S. performed research; M.S. and M.J.M. contributed new reagents/analytic tools; G.M. and S.C. analyzed data; and G.M., J.C.K., and S.C. wrote the paper.

The authors declare no competing interest.

This article is a PNAS Direct Submission.

[1]To whom correspondence may be addressed. Email: shukti.chakravarti@nyumc.org.

This article contains supporting information online at https://www.pnas.org/lookup/suppl/doi:10.1073/pnas.2100999118/-/DCSupplemental.

Published July 2, 2021.

that are likely cryptic due to their associations with collagen fibrils in homeostatic ECMs (25, 26). Indeed, SLRP fragmentations reported in inflamed arthritic tissues (27) and possibly other ECM tissues during injury and repair, can increase cross-talks of various SLRP epitopes with immune cell receptors that are yet to be deciphered.

The TLRs unleash formidable immune responses against a variety of pathogens at the cell surface and specific endosomal locations (28, 29). TLR-1, -2, -4, -5, and -6 recognize microbial components at the cell surface, and the endosomal TLRs, namely TLR-3, -7, -8, -9, and -13, recognize microbial nucleic acids released in the acidic environment of endolysosomes. TLRs are highly regulated by their location, processing, accessory proteins, and ligand encounter to control inflammation and stave off autoimmune responses (30, 31). TLR4 recognizes lipopolysaccharides (LPS) at the cell surface in lipid-rich microdomains to drive MyD88-dependent induction of proinflammatory cytokines. LPS-induced endocytosis takes TLR4 to early endosomes, where it recognizes endosomal LPS to induce MyD88-independent proinflammatory cytokines and type I interferon (28). CD14, structurally related to TLRs (32), is an important mediator of TLR4 signaling (33). CD14 presents LPS to the TLR4-MD2 complex at the cell surface (34–36), is essential for trafficking of TLR4 to endosomes (37, 38), and is essential for the endosomal response to LPS (39). Among endosomal nucleic acid sensors, TLR9 responds to microbial DNA and the synthetic ligand CpG oligonucleotide in endolysosomes (40). CD14 also aids TLR9 in its response to DNA and MyD88-dependent induction of proinflammatory cytokines and type I interferons (41). Caveolin 1 (Cav1), a major component of caveolae, regulates endocytosis of pathogens, lipids, and proteins at lipid-rich sites of the plasma membrane (42), affecting TLR responses (43) and as our findings show, has a specific role in ECM–immune cell interactions.

We demonstrate that Lum, secreted by inflammation-activated fibroblasts, promotes TLR4 but restricts TLR9 signals in macrophages and dendritic cells (DCs). A common mechanism of receptor and ligand compartmentalization by Lum is implicated in these seemingly divergent functions. Lum interacts with CD14 and Cav1 through two distinct sites to enrich these and TLR4 in plasma membrane lipid rafts to promote proinflammatory signals at the cell surface. Endocytosed Lum maintains TLR4 and LPS proximity in signal-permissive endosomes to aid type I interferon production. Endosomal Lum delays TLR9 trafficking and competes with CD14 to bind and sequester CpG DNA to dampen TLR9 response. Bgn also binds CpG DNA and suppresses TLR9 response, but it does not bind Cav1 or contribute to surface presentation of Cav1, CD14, and TLR4. The ECM SLRPs may thus have shared and unique roles in regulating cell surface and endosomal TLR functions. Consistently, $Lum^{-/-}$ mice challenged with polymicrobial sepsis show poor TLR4-mediated proinflammatory cytokine response, impaired bacterial clearance, and increased circulating anti-DNA antibodies. We detected elevated Lum in sepsis patients' plasma, while human peripheral blood monocytes (PBMCs) treated with recombinant Lum show elevated TLR4 but suppressed TLR9 responses as in our mouse studies. Our findings will impact how we envision the ECM in shaping bacterial and viral immunity and autoimmunity beyond the cell surface as regulators of intracellular trafficking in immune cells.

Results

A Protective Role for Lumican in Sepsis from Human and Mouse Studies. We measured the abundance of Lum in the plasma of 11 sepsis and 17 healthy individuals (Fig. 1*A*) and found a small but consistent increase in sepsis patients (26.41 ± 1.54 ng/mL versus 21.0 ± 1.19 ng/mL). We next tested the effects of exogenous recombinant lumican (rLum) on LPS-stimulated PBMCs from healthy volunteers and observed increased secretion of TNF-α and IFN-α in the presence of rLum, indicating a signal-enhancing role for Lum in TLR4 response in humans (Fig. 1*B*). In contrast to its effects on LPS response, rLum suppressed IFN-α and IFN-β induction in response to CpG DNA by TLR9 in human PBMC (Fig. 1*C*).

To further investigate the role of Lum in TLR signals in sepsis, we used a mouse model of cecal slurry–induced polymicrobial sepsis (CIP) (44) in $Lum^{-/-}$ and wild-type (WT) or $Lum^{+/-}$ mice as Lum-positive controls (Fig. 1*D*). After an intraperitoneal injection of cecal slurry, we followed disease outcomes for 4 d, when Lum increases in sera and peritoneal lavage of CIP-treated Lum-positive mice (Fig. 1*E*). The CIP-challenged $Lum^{-/-}$ mice show greater body weight loss (Fig. 1*F*), poor bacterial clearance from the peritoneum (Fig. 1*G*), and higher bacterial load in the blood stream at day 4 (Fig. 1*H*), indicative of worse systemic disease in the $Lum^{-/-}$ compared with Lum-positive mice. Of note, only aerobic bacteria were assayed here, although the mouse gut is known to host a range of anaerobic bacteria as well. Furthermore, on day 4, the $Lum^{-/-}$ mice show lower circulating proinflammatory cytokines TNF-α, IL-6, IL-12, CCL2, and IL-1β (Fig. 1 *I–M*). Consistently, early (day 1) infiltration of macrophages, neutrophils, monocytes, and DCs is lower in the peritoneal lavage of $Lum^{-/-}$ compared with $Lum^{+/-}$ mice (*SI Appendix*, Fig. S1 *A–G*).

In contrast to the decrease seen in TLR4-mediated proinflammatory cytokines, we detected increased pIRF7 in peritoneal extracts of CIP-challenged $Lum^{-/-}$ mice, consistent with increased TLR9 signals in these compared with WT mice (Fig. 1*N*). Moreover, circulating anti-DNA IgG (*SI Appendix*, Fig. S1*H*) and antinucleosome IgG (*SI Appendix*, Fig. S1*I*), which involves TLR9 signals, were elevated in 4-d CIP-challenged $Lum^{-/-}$ mice. As infections can trigger anti-DNA antibodies through TLR9 signals in humans as well (45, 46), we tested sepsis patients' plasma and detected a negative correlation between anti-DNA antibodies and circulating Lum levels (*SI Appendix*, Fig. S1 *J* and *K*). However, a larger sample size is needed to draw statistically significant conclusions. Taken together, these observations suggest a role for Lum in promoting TLR4 and restricting TLR9 responses in sepsis.

Paracrine Source of Lumican from Peritoneal Omentum Fibroblast. Lum is clearly induced under inflammatory conditions, as evidenced here by its increase in sepsis patients' plasma and in our previous studies on inflammatory bowel disease and bacterial infections of the mouse cornea (16, 22). Yet, Lum, normally expressed in mouse embryonic fibroblasts (MEF) and TNF alpha–activated fibroblasts (47), is undetectable by qPCR in peritoneal macrophages (pMacs), $CD11c^{+}$ DCs, and the mouse macrophage–like RAW 264.7 cells (Fig. 2*A*). Moreover, the Lum core protein, not detectable in RAW 264.7 cell extracts, is detectable in freshly isolated WT pMacs and lost in acid-wash stripped cells (Fig. 2*B*), implying that Lum secreted by other cell types associate with the macrophage cell surface. To identify important cellular sources of Lum, we considered adult tissue fibroblasts. A likely source of the pMac-pericellular Lum is fibroblasts of the omentum, a membranous ECM-rich fatty tissue in the peritoneal cavity (48). Cultured omentum fibroblasts (OmFb) (*SI Appendix*, Fig. S2) from WT mice ($Lum^{-/-}$ mice OmFb used as a negative control) secrete Lum constitutively, which increases further after treatment with TNF-α or IL-1-β, MEF by comparison secrete less Lum (Fig. 2*C*). Conditioned medium (CM) from WT OmFb increases LPS response and TNF-α induction in $Lum^{-/-}$ pMacs, while $Lum^{-/-}$ OmFb CM does not (Fig. 2*D*). Also, the exogenous, adherent Lum gets diluted in culture over time (Fig. 2*E*), and as expected, there is a temporal decrease in LPS-induced TNF-α in WT pMac cultures (Fig. 2*F*). Based on these observations, we propose that Lum secreted by fibroblasts exert its paracrine effects on pMacs to promote TLR4 signals, and proinflammatory cytokines released by pMacs in turn activate fibroblasts in a feed-forward loop (Fig. 2*G*).

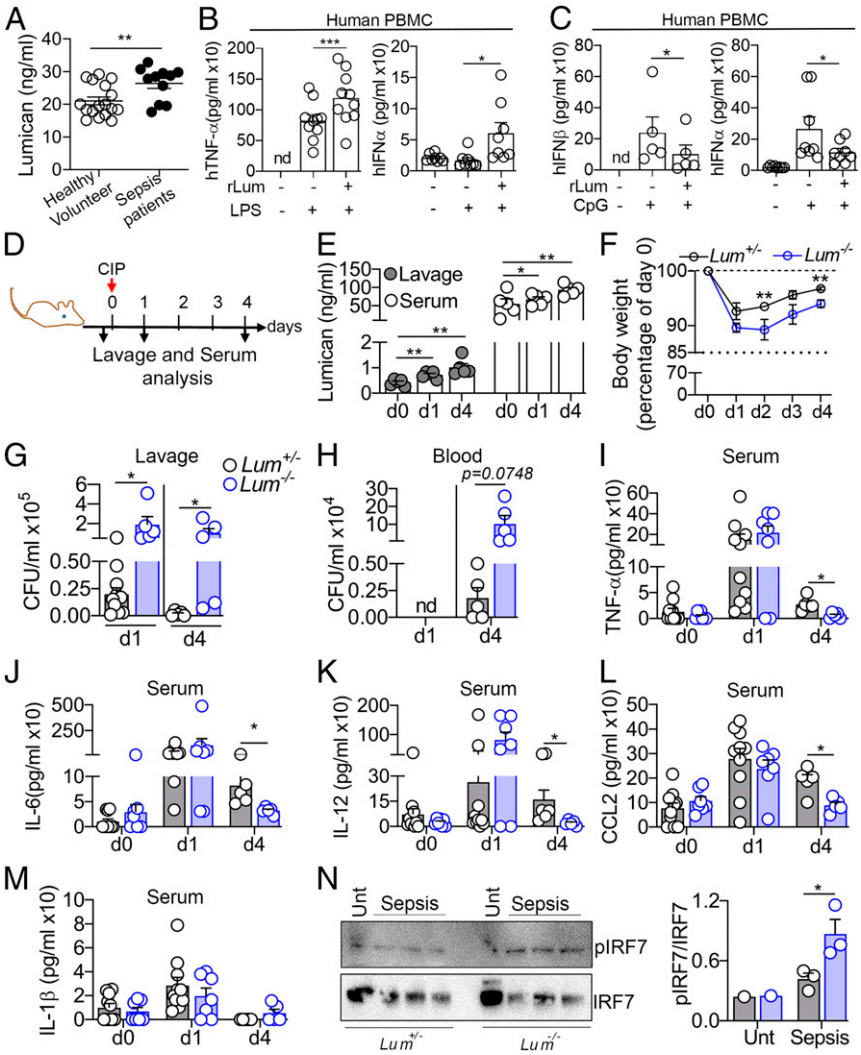

Fig. 1. Lumican is involved in human sepsis and regulates polymicrobial sepsis in a mouse model. (*A*) Increased Lum levels (ELISA) in sepsis patients' plasma compared with healthy volunteers. (n = 11 to 17). (*B* and *C*) Healthy human PBMCs pretreated with rLum (10 μg/mL) for 1 h and stimulated with LPS (100 ng/mL) or CpG DNA (1 μM) for 6 h. TNF-α and IFN- α levels were estimated by ELISA (n = 8 to 10 human samples from four independent experiments). (*D*) CIP in mice. (*E*) Lavage and serum Lum at day 0, 1, and 4 after CIP measured by ELISA. (*F*) Body weight as a percentage of weight on day 0 in $Lum^{+/-}$ and $Lum^{-/-}$ CIP mice. (*G* and *H*) Bacterial colony-forming unit (CFU) in peritoneal lavage and blood from $Lum^{+/-}$ and $Lum^{-/-}$ after CIP. (*I–M*) Serum cytokine levels after CIP by multianalyte flow assay kit. (*N*) p-IRF7 and IRF7 immunoblot of peritoneal cell lysates of day 4 CIP mice. The bar graph shows the densitometric analysis. Each data point represents one mouse. One of two independent experiments. n = 5 to 10 mice/genotype from three independent experiments shown in *G–M*. Significance was determined by two-tailed unpaired Student's t test (*A–C*) and two-way ANOVA with Sidak's multiple comparison posttest (*G–M*). $^*P < 0.05$, $^{**}P < 0.01$, and $^{***}P < 0.001$. The error bars represent SEM.

Lumican Promotes Both Cell Surface MyD88-Dependent and Endosomal MyD88-Independent TLR4-Signaling Axes. To investigate the molecular mechanisms underlying the TLR4-promoting functions of Lum, we tested its involvement in the two TLR4-signaling axes, firstly, the cell surface TLR4-MyD88-TNF-α, and secondly, the MyD88-independent endosomal TLR4-TRIF/TRAM-type I interferon induction (28). $Lum^{-/-}$ mouse pMacs, stimulated with LPS, show lower induction of TNF-α, IL-1-β, and IL-6 compared with $Lum^{+/+}$ (W T) pMacs, supporting a positive role for Lum in the cell surface TLR4-signaling axis (Fig. 3 *A–C*). Lum also promotes the endosomal TLR4-signaling axis, as $Lum^{-/-}$ pMacs produce significantly lower IFN-β than WTs after 18 h of LPS treatment (Fig. 3*D*). Corroboratively, nuclear translocation of the NF-κB p65 subunit (downstream of both axes) and induction of cytoplasmic pIRF3 (a result of endosomal TLR4 signaling) are also lower in $Lum^{-/-}$ compared with WT pMacs (Fig. 3*E*). In the same vein, rLum increases TLR4 signals in LPS-stimulated RAW 264.7 cells as evident from the increase in pERK1/2 and p-p38 (Fig. 3*F*). Moreover, myddosome complex formation, determined by coimmunoprecipitation (co-IP) of MyD88 and IRAK4, occurs more rapidly (by at least 30 min) in *Lum* transgene–expressing RAW 264.7 cells compared with those carrying the empty vector (Fig. 3*G*), although Lum does not directly bind to the myddosome complex. Taken together, these experiments identify a positive role for Lum in the cell surface and the endosomal TLR4-signaling axes to induce inflammatory cytokines and IFN-β, respectively.

We further investigated the macrophage transcriptome from WT and $Lum^{-/-}$ mice and detected a stronger, classically activated M1 phenotype (*Tnfa*, *Tank*, *Il6*, *Stat1*, *Socs3*) in WT compared with $Lum^{-/-}$ pMacs, while exogenous rLum increased *Il12b* and suppressed *Il15*, *Il18*, *Stat1*, and *Socs3* expression in LPS-stimulated pMacs (*SI Appendix*, Fig. S3*A*). Multiple TLRs are induced after LPS treatment, but *Lum* deficiency has no marked effect on *Tlr* gene expressions (*SI Appendix*, Fig. S3*B*).

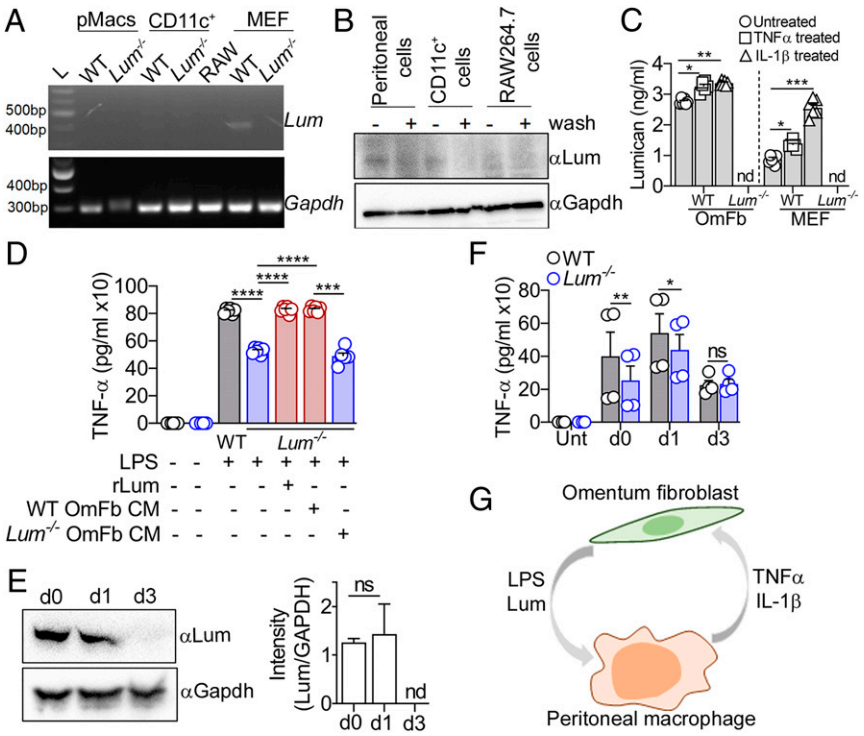

Fig. 2. OmFb-secreted lumican exerts paracrine regulation on macrophages. (*A*) *Lum* and *Gapdh* expression by semi-qPCR from WT and *Lum*$^{-/-}$ (negative control) pMacs, CD11c^{+} cells, and MEF. One of three independent experiments. (*B*) Immunoblot showing cell-associated Lum in WT pMacs, CD11b^{+} cells, and RAW264.7 cells before and after acidic (pH 2.2) wash; Gapdh used as a protein loading control. One of two independent experiments. (*C*) OmFb and MEF from WT and *Lum*$^{-/-}$ untreated or treated with TNF-α or IL-1β for 48 h, and Lum secreted was quantified by ELISA. ($n = 6$ technical replicates from three independent experiments). (*D*) TNF-α by ELISA in the culture media of pMacs untreated or pretreated with CM from HEK293 cell expressing the *rLum* transgene, or CM from WT OmFb, or *Lum*$^{-/-}$ OmFb for 1 h followed by LPS for 6 h ($n = 6$ technical replicates from three independent experiments). (*E*) Immunoblot of endogenous Lum associated with WT and *Lum*$^{-/-}$ pMacs in cell extracts harvested immediately (d0) or after one (d1) or 3 d (d3) in culture. One of two independent experiments. (*F*) ELISA of TNF-α secreted by LPS-stimulated pMacs on d0, d1, or d3 in culture ($n = 4$ technical replicates from two independent experiments). (*G*) A schematic representation of positive feed-forward signaling between OmFb and pMACs. Lum secreted by OmFb enhances proinflammatory cytokines (TNF-α and IL-1β) production by pMacs upon LPS stimulation. Significance determined by a two-way ANOVA (*D* and *E*) and two-tailed Student's *t* test (*F* and *G*). *$P < 0.05$, **$P < 0.01$, ***$P < 0.001$, ****$P < 0.0001$, and ns, not significant; nd, not detected. The error bars represent SEM.

Lumican Promotes TLR4 Enrichment at the Cell Surface. Since our data implicates a positive role for Lum in TLR4 signals from the cell surface and endosomes, we questioned whether it does so by preserving TLR4 levels in these signal-permissive compartments. We examined surface TLR4 and CD14 on pMacs by flow cytometry. Of the entire population of peritoneal cells, 3.93 ± 0.49% are TLR4 positive in *Lum*$^{-/-}$ compared with 9.89 ± 0.79% in WT (Fig. 4 *A* and *B*) and a 25% decrease in TLR4 mean fluorescence intensity (MFI) in the former (Fig. 4*C* and *SI Appendix*, Fig. S4*A*). Gated on CD11b^{+} cells, 12.5 ± 0.8% are TLR4 positive in *Lum*$^{-/-}$ compared with 33 ± 2% in WTs (*SI Appendix*, Fig. S4 *B* and *C*). Notably, incubation with rLum increases TLR4^{+} cells (Fig. 4*B*) and restores TLR4 MFI to WT levels in *Lum*$^{-/-}$ pMacs (Fig. 4*C* and *SI Appendix*, Fig. S4*A*). The *Lum*$^{-/-}$ peritoneal cells also have lower surface CD14 (34 ± 3% of total and 71 ± 4% of CD11b+ cells) compared with WTs (40 ± 0.7% of total, and 96 ± 1% CD11b^{+} peritoneal cells) (*SI Appendix*, Fig. S4 *D–F*), and rLum can restore these to WT levels (Fig. 4*D* and *SI Appendix*, Fig. S4 *E–G*). Most notably, rLumY20A, which does not bind CD14 (21), is unable to restore surface TLR4 or CD14 to WT levels (Fig. 4*E* and *SI Appendix*, Fig. S4*H*). The mutant rLumY20A is also unable to restore the TNF-α induction functionality in *Lum*$^{-/-}$ pMacs to WT levels (Fig. 4*F*). Similarly, rLumY20A is unable to increase nuclear translocation of NF-κB p65 in LPS-stimulated RAW 264.7 cells (*SI Appendix*, Fig. S4*I*). Therefore, rLumY20A provides a genetic link between the abundance of CD14 and TLR4 at the plasma membrane and LPS-induced cytokine expression.

CD11b^{+} pMacs from WT, *Lum*$^{-/-}$, and *Bgn*$^{-/-}$, included as another non-Lum SLRP, show comparable levels of *Tlr4*, *Tlr9*, *Cd14*, and *Cav1* transcripts, and of these, only *Cd14* is markedly inducible by LPS (Fig. 4 *G* and *H*, additional global transcriptomic data in *SI Appendix*, Fig. S3 and the raw data in Gene Expression Omnibus [GEO], accession no. GSE174026). Several downstream mediators of TLR4 signal (*Myd88*, *Traf6*, *Irak3*, *Nfkb1*, *Irf7*, and others) are elevated comparably in LPS-treated *Lum*$^{-/-}$ and WT pMacs (*SI Appendix*, Fig. S3*B*). Together, these findings underscore a direct posttranscriptional regulation of TLR4 and its signal intermediates by Lum, although there are consequential transcriptional changes in other inflammation-related genes.

After LPS encounter, TLR4 and CD14 are known to be internalized, reducing their cell surface levels (49). To determine whether Lum regulates the rate of LPS-induced receptor endocytosis, we used flow cytometry to measure the temporal loss of surface TLR4 and CD14 from LPS-treated WT and *Lum*$^{-/-}$ pMacs. The rates of surface TLR4 and CD14 loss are similar in *Lum*$^{-/-}$ and WT, and internalization rates are unaffected by exogenous rLum (*SI Appendix*, Fig. S5 *A* and *B*). As Bgn is reportedly a TLR4 ligand itself (23), we asked whether, like Lum, it also promotes TLR4 response by helping to retain cell surface TLR4. However, levels of surface TLR4 and CD14 (*SI Appendix*, Fig. S5 *C* and *D*) on *Bgn*$^{-/-}$ pMacs are no different from WT, indicating a lack of Bgn involvement in CD14 and TLR4 compartmentalization.

We next sought to define the biochemical basis for Lum-mediated enhancement of cell surface TLR4 and CD14. Membrane extracts

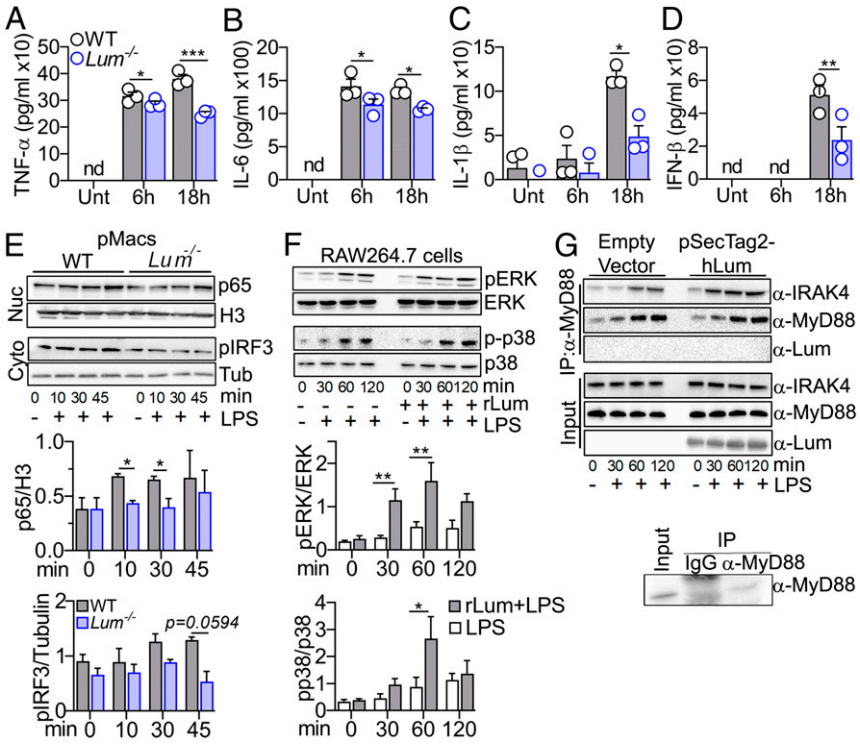

Fig. 3. Lumican promotes cell surface and endosomal TLR4 signals in macrophages. (*A–D*) WT and *Lum*$^{-/-}$ pMacs were stimulated with LPS (100 ng/mL) for 6 or 18 h and secreted TNF-α (*A*), IL-6 (*B*), IL-1β (*C*) and IFN-β (*D*), measured by ELISA in three mice/genotype from three independent experiments shown as mean ± SEM. (*E*) Immunoblots of p65 (nuclear) and pIRF3 (cytoplasmic) in elicited pMacs from WT and *Lum*$^{-/-}$ treated with LPS. (*F*) Immunoblots of p-ERK1/2, ERK, p-p38, and p38 in extracts of LPS-treated RAW264.7 cells pretreated with or without rLum. The bar graphs show densitometry scans for *E* and *F*. (*G*) Immunoprecipitation (IP) of MyD88 and IB of IRAK4 and Lum to detect myddosome complex in LPS-stimulated expressing rLum or empty vector control RAW264.7 cells. MyD88 is absent in the control IgG IP. The images (*E–G*) are representative of two to three independent experiments. For *A–D*, statistical significance was determined by two-tailed unpaired Student's *t* test. *$P < 0.05$, **$P < 0.01$, ***$P < 0.001$, and nd, not detected.

from untreated and LPS-treated pMacs fractionated by sucrose-gradient density centrifugation and immunoblotted for TLR4 show a marked decrease in TLR4 in the *Lum*$^{-/-}$ pMac lipid raft fractions (Fig. 4*I*), consistent with the lower surface TLR4 detected by flow cytometry. We used Cav1 as a lipid raft marker, and unexpectedly, this revealed a dramatic decrease in Cav1 in raft fractions of *Lum*$^{-/-}$ compared with WT pMacs (Fig. 4*I*). In agreement, we observed Cav1, TLR4, and CD14 enrichment in lipid raft fractions of RAW 264.7 cells treated with LPS and rLum compared with those treated with LPS alone (*SI Appendix*, Fig. S5*E*). We considered a reciprocal need for Cav1 to maintain Lum on cell surfaces. Indeed, *Cav1*$^{-/-}$ pMac cell extracts carry half as much Lum as WT pMacs (*SI Appendix*, Fig. S5*F*), although peritoneal lavage supernatants of WT and *Cav1*$^{-/-}$ mice have comparable levels of soluble Lum (*SI Appendix*, Fig. S5*G*). We visualized lipid rafts with fluorescently tagged Cholera toxin B that show diffused staining of rafts on *Lum*$^{-/-}$ compared with WT pMacs, supporting a link between raft integrity and Lum (*SI Appendix*, Fig. S5*H*). However, immuno-dot blots show that Lum does not directly bind to plasma membrane lipids (*SI Appendix*, Fig. S5*I*).

Lumican Binds and Promotes Cell Surface Presentation of Cav1. In support of Cav1 enrichment by Lum in lipid rafts, we detected a significant decrease in surface Cav1 (96 ± 8.72 MFI) on *Lum*$^{-/-}$ compared with WT pMacs (115 ± 19.3 MFI) (Fig. 5*A* and *SI Appendix*, Fig. S6*A*). *Bgn*$^{-/-}$ pMacs on the other hand, show WT levels of surface Cav1, indicating a lack of Bgn-mediated regulation of surface Cav1 (*SI Appendix*, Fig. S6*B*). Incubation of *Lum*$^{-/-}$ pMacs with exogenous rLum rescued surface Cav1 to WT levels (Fig. 5*B*). Concordantly, both HEK 293T and RAW 264.7 (*SI Appendix*, Fig. S6 *C* and *D*) cells show dose-dependent increase in surface Cav1 in the presence of increasing concentrations of rLum in the culture medium. Interestingly, Y20ArLum, which does not bind or rescue surface CD14 and TLR4, is still able to restore surface Cav1 levels in *Lum*$^{-/-}$ pMacs (Fig. 5*B* and *SI Appendix*, Fig. S6*E*). Thus, the surface Cav1-restoring site is independent of the CD14-binding Y20 site in the Lum protein. By surface plasmon resonance (SPR), we detected strong binding (equilibrium dissociation constant [KD] = 1.27×10^{-12} M; equilibrium association constant [KA] = 7.88×10^{11} M^{-1}) between rLum and Cav1 (Fig. 5*C* and *SI Appendix*, Fig. S6*F*). rBgn and rDcn do not bind Cav1 (*SI Appendix*, Fig. S6 *G* and *H*), though they do bind CD14 (*SI Appendix*, Fig. S6 *I* and *J*). Lum and Cav1 co-IP from HEK 293T cells expressing the *Lum* and *Cav1* transgenes (Fig. 5*D*), and in a more physiological setting, the endogenous proteins from peritoneal lavage cells of WT mice (Fig. 5*E*), validating Lum-Cav1 binding in vivo. The Cav1 binding consensus sequences include ØXØXXXXØ and ØXXXXØXXØ, where Ø is an aromatic and X any amino acids (50). Therefore, the YFKRFNALQY sequence in the LRR 7 to 8 motif of Lum is a good candidate for Cav1 interactions. We expressed a mutated F228ArLum, where the second phenylalanine (F) is changed to alanine (A) (Fig. 5*F*). In transgene-expressing HEK293T cells, F228ArLum and Cav1 do not co-IP, supporting the F228A mutation to cause loss of Cav1 binding in rLum (Fig. 5*G*). Furthermore, F228ArLum or one where FKRF are all changed to A residues (A225 to 228) (Fig. 5*F*) are unable to recover surface Cav1 to WT levels (Fig. 5*H* and *SI Appendix*, Fig. S6*K*). We next tested F228ArLum for its ability to restore surface TLR4 and CD14 in *Lum*$^{-/-}$

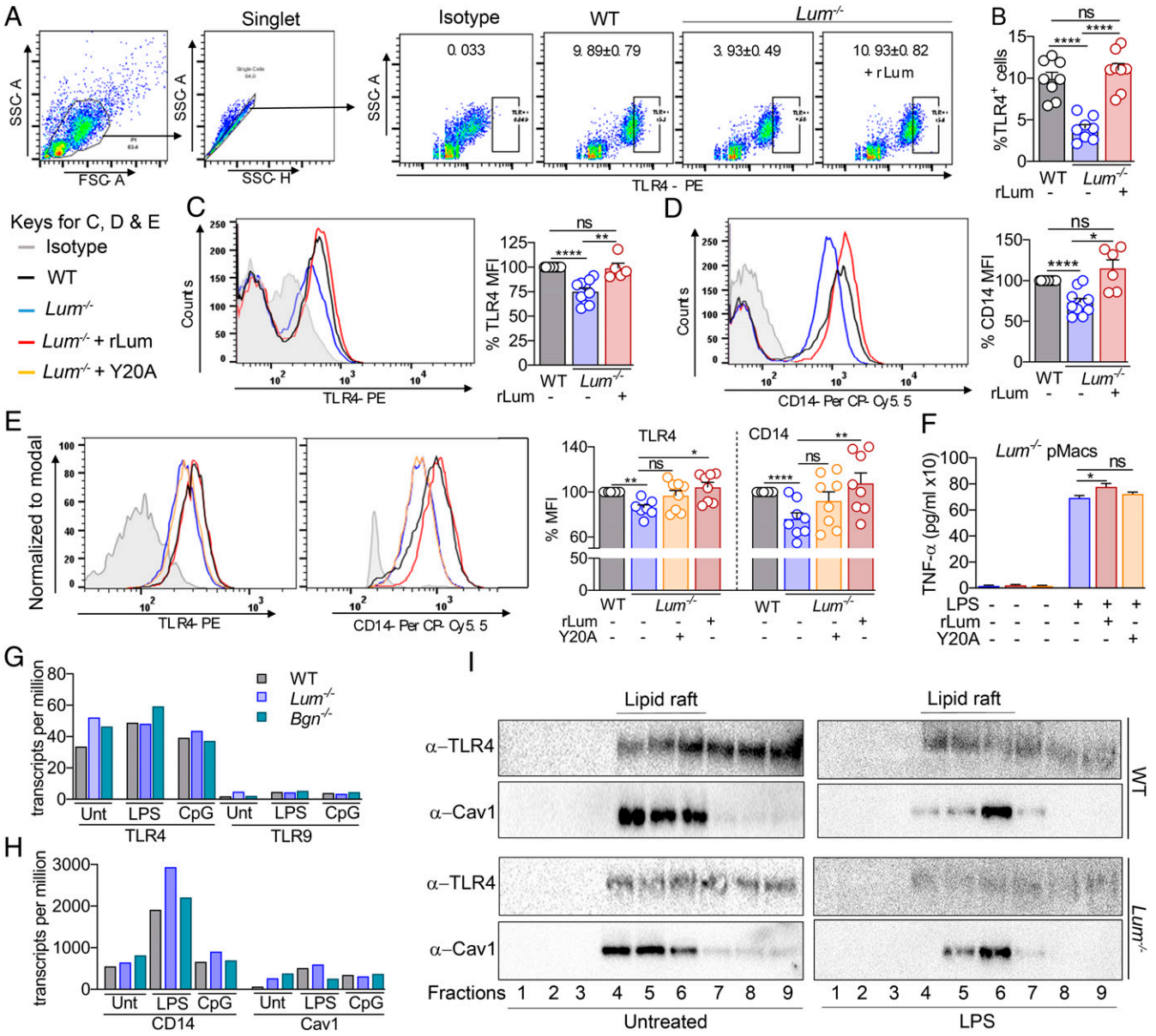

Fig. 4. Lumican increases TLR4 and CD14 at the cell surface and TLR4 response in pMacs. (*A* and *B*) Surface TLR4 on WT and *Lum*$^{-/-}$ pMacs treated with rLum for 1 h and stained with TLR4-PE. (*A*) Gating scheme and representative dot plots. (*B*) Percentage of TLR4+ peritoneal cells ($n = 3$ independent experiments). (*C*) A representative histogram of WT and *Lum*$^{-/-}$ pMacs stained with TLR4- PE. Cumulative data shows percent geometric MFI of surface TLR4 ($n = 5$ to 10 mice/genotype from three independent experiments). (*D*) A representative histogram of WT and *Lum*$^{-/-}$ pMacs stained with CD14–PerCP-Cy5.5. Cumulative data shows percent MFI of surface CD14 ($n = 6$ to 12 mice/genotype from three independent experiments). (*E*) A representative histogram of TLR4–PE and CD14–PerCP-Cy5.5 on WT and *Lum*$^{-/-}$ pMacs, treated with rLum or mutated rLum Y20A–conditioned media (Y20A) for 1 h ($n = 7$ to 8 technical replicates from two independent experiments). (*F*) *Lum*$^{-/-}$ pMacs pretreated with rLum or Y20A and LPS for 6 h. TNF-α quantified by ELISA ($n = 6$ technical replicates from two independent experiments). (*G* and *H*) Gene expression in transcripts per million of *Tlr4* and *Tlr9* (*H*) and *Cd14* and *Cav1* (*I*) from RNA sequencing of purified CD11b^{+} WT, *Lum*$^{-/-}$, and *Bgn*$^{-/-}$ cells untreated or treated with LPS or CpG DNA for 6 h. (*I*) Immunoblot of TLR4 and Cav1 proteins in fractions from sucrose-density gradient ultracentrifugation of WT and *Lum*$^{-/-}$ pMac extracts, untreated or pretreated with rLum for 1 h and LPS for 6 h. One of two independent experiments. Statistical significance by two-way ANOVA (*B–F*) and two-tailed unpaired Student's *t* test (*F*). *$P < 0.05$, **$P < 0.01$, ****$P < 0.0001$, and ns, not significant. The error bars represent SEM.

pMacs; F228ArLum recovered surface CD14 but not surface TLR4 (Fig. 5*I* and *SI Appendix*, Fig. S6*L*). Also, F228ArLum failed to recover the induction of TNF-α in *Lum*$^{-/-}$ pMacs after LPS stimulation (Fig. 5*J*). Cumulatively, these results suggest that Cav1 binding, and its surface presentation by Lum, resides in its F228 region and is not critical for binding or keeping surface CD14, but that both F228 and the Y20 epitopes in Lum are required for surface presentation of TLR4 and its TNF-α response to LPS at the cell surface.

Endocytosed Lumican Promotes TLR4 Compartmentalization in Signal-Permissive Endosomes. Since endosomal TLR4 signal is promoted by Lum, we asked whether extracellular Lum is endocytosed by immune cells; fluorescently tagged rLum (Alexa Fluor 488-rLum) is taken up by pMacs (Movie S1) and DC (*SI Appendix*, Fig. S7*A*) within an 1 h in culture. Flow cytometry of WT peritoneal lavage cells incubated with His-tagged rLum (His-rLum) indicate 42 ± 2% of F4/80^{+} cells are positive for His-rLum (Fig. 6 *A* and *B* and *SI Appendix*, Fig. S7*B*). Filipin, an inhibitor of caveolar

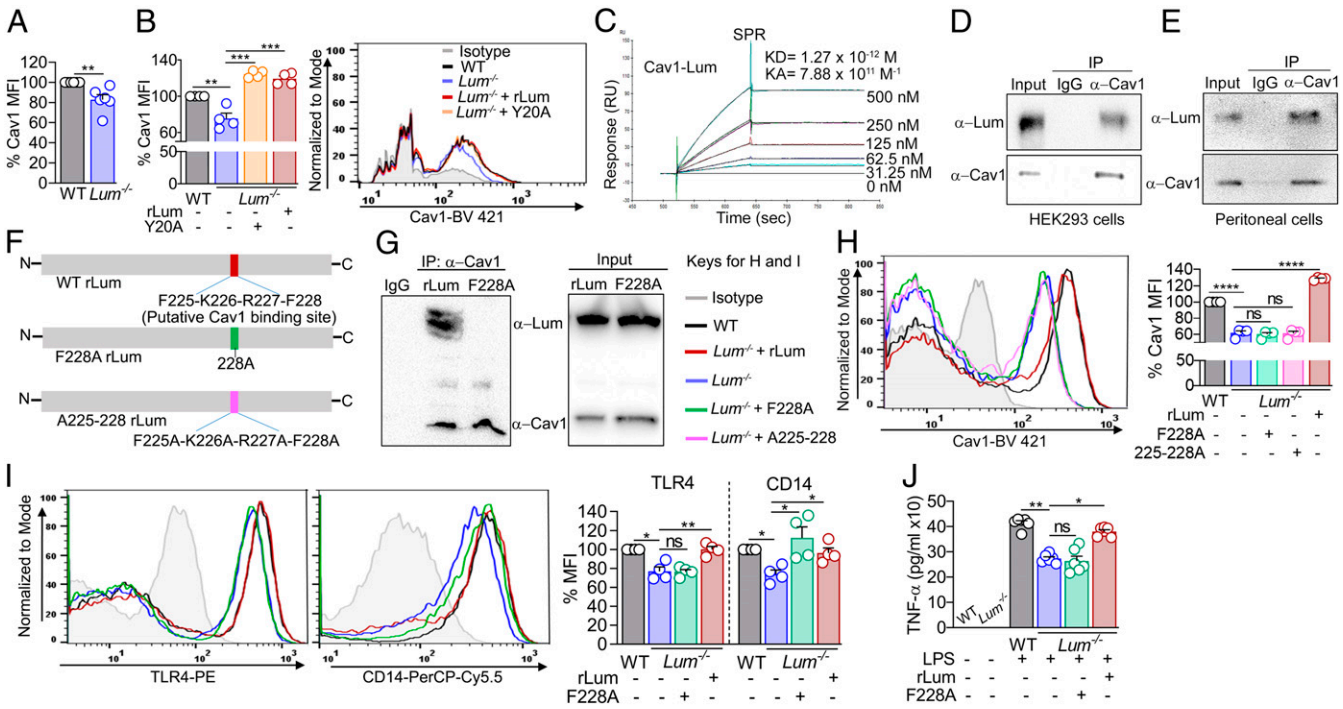

Fig. 5. Lumican binds and enriches surface Cav1 on pMacs. (*A*) Basal surface Cav1 by flow cytometry on WT and *Lum*$^{-/-}$ pMacs (n = 6 to 7 mice/genotype from three independent experiments). (*B*) Representative histograms of WT and *Lum*$^{-/-}$ pMacs stained with Cav1-BV421. Cumulative data shows surface Cav1 on pMacs treated with rLum or Y20A for 1 h (n = 4 to 6 mice/genotype from two independent experiments). (*C*) Sensorgram measurements of Lum and Cav1 binding by SPR. (*D*) co-IP of rLum-Cav1 from HEK 293T cells transiently expressing Cav1 and rLum. Negative control—IP with nonspecific IgG. The image shown is one of two independent experiments. (*E*) co-IP of endogenous Lum-Cav1 from elicited WT pMac extracts. One of two independent experiments. (*F*) rLum, mutated F228A rLum and F225-228A rLum constructs. (*G*) co-IP of Cav1 and rLum or F228A rLum from transgene-transfected HEK 293T cells after 52 h in culture. The image shown is one of two independent experiments. (*H*) Representative histograms of WT and *Lum*$^{-/-}$ pMacs stained with Cav1-BV421. Cumulative data shows surface Cav1 on WT and *Lum*$^{-/-}$ pMacs treated with conditioned media containing rLum or F228ArLum (F228A) or rLum 225 to 228A (225 to 228A) for 1 h (n = 4 technical replicates from two independent experiments). (*I*) A representative histogram of WT and *Lum*$^{-/-}$ pMacs treated with rLum or F228A rLum CM for 1 h, stained with TLR4–PE and CD14–PerCP-Cy5.5. Cumulative data shows surface TLR4 and CD14 (n = 3 to 4 technical replicates from two independent experiments). (*J*) Secreted TNF-α (ELISA) in WT and *Lum*$^{-/-}$ pMacs pretreated with CM from HEK293 cells expressing rLum or F228A, followed by LPS for 6 h (n = 6 technical replicates from three independent experiments). Significance determined by two-way ANOVA (*B*, *H*, *I*, and *J*) and two-tailed Student's t test (*A*). *P < 0.05, **P < 0.01, ***P < 0.001, ****P < 0.0001, and ns, not significant. The error bars represent SEM.

endocytosis, results in a 10-fold decrease in F4/80$^+$ His-rLum$^+$ cells, while chlorpromazine, an inhibitor of clathrin-mediated endocytosis, cause a fourfold decrease. Thus, caveolar endocytosis is the dominant route, although both mechanisms support Lum uptake. Caveolar uptake of Lum is further validated by our observation that *Cav1*$^{-/-}$ show almost 50% reduction in rLum uptake compared with WT pMacs (n = 5 to 6 mice) (*SI Appendix*, Fig. S7*C*). In step with these observations, confocal microscopy of pMacs show colocalization of exogenous His-tagged rLum with Cav1 as well as transferrin, a known cargo for clathrin-mediated endocytosis (Fig. 6*C*). We next tested vesicular trafficking of His-tagged rLum in WT pMacs (to use a WT vesicular transport setting). Within 1 h, rLum colocalizes with early (Rab5 and VAMP3), recycling (Rab11), and late (Rab7) endosome markers as well as the endolysosome marker, LAMP1 (Fig. 6*D*). We further determined whether Lum colocalizes with TLR4 and LPS within endocytic vesicles. WT pMacs incubated with His-tagged rLum and fluorescently tagged (FITC) LPS show robust colocalization of Lum with both LPS and TLR4 (Fig. 6*E*), demonstrating that, after endocytosis, Lum travels through vesicles harboring LPS and TLR4.

We examined whether Lum regulates endosomal locations of TLR4 in pMacs. Within 20 min after LPS exposure, *Lum*$^{-/-}$ pMacs show lower TLR4 staining in EEA1$^+$ early endosomes, and by 60 min, this is significantly lower than WT (Fig. 7*A*). We also compared the trafficking of TLR4 with LAMP1$^+$ endolysosomes between 0 and 120 min after LPS treatment and found significantly higher TLR4 in LAMP1$^+$ endolysosomes in *Lum*$^{-/-}$ (66 to 77 cells analyzed) compared with WT pMacs (Fig. 7*B*). Thus, in the absence of Lum, TLR4 travels to endolysosomes faster, likely for rapid degradation and turnover. This is consistent with our biochemical data that indicate lower TLR4 levels in lipid-rich membrane fractions of *Lum*$^{-/-}$ as compared with WT pMacs.

Lumican Suppresses TLR9 Response by Regulating CpG DNA and TLR9 Trafficking. Consistent with TLR9 suppression by rLum in human PBMC, *Lum*$^{-/-}$ pMacs show significantly higher than WT induction of TNF-α (Fig. 8*A*) and expression of *Tnfa*, *Ifnb1*, and its target *Cxcl10* in response to CpG DNA (Fig. 8*B*), while exogenous rLum lowers the induction of TNF-α (Fig. 8*C* and *SI Appendix*, Fig. S8*A*). Of note, CD14 is known to help TLR9 signal propagation (41), and as expected, TNF-α induction by CpG DNA is drastically reduced in *CD14*$^{-/-}$ pMacs (Fig. 8*A*). Also, just as the TLR4 response in WT versus *Lum*$^{-/-}$ is equalized after culturing, the differential TNF-α induction by TLR9 is abrogated by 1 to 3 d in culture due to the eventual loss of surface-associated Lum (*SI Appendix*, Fig. S8*B*). Testing additional nodes in TLR9 signaling, exogenous rLum reduces phospho ERK1/2 in CpG DNA–stimulated RAW 264.7 cells (*SI Appendix*, Fig. S8*C*). Interestingly, mutated Y20ArLum and F228A rLum, which are inactive in maintaining surface CD14 and Cav1, respectively, and restoring TLR4 response, are completely functional in suppressing TLR9 response in pMacs in culture (Fig. 8*C*). This indicates that interactions with CD14 and Cav1 may not be needed for Lum to engage

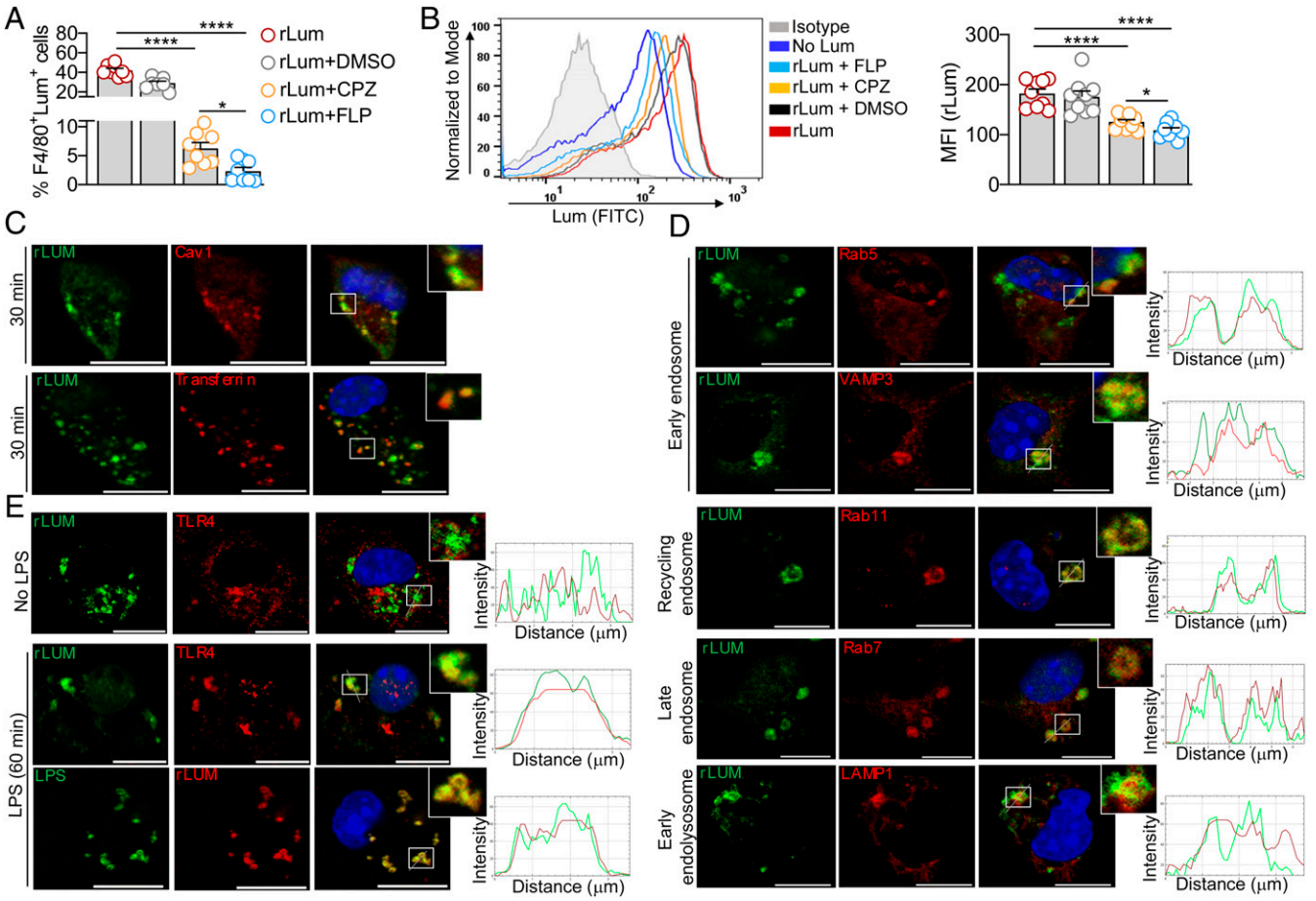

Fig. 6. Lumican endocytosed by pMacs promotes TLR4 compartmentalization in signal-permissive endosomes. (*A*) His-tagged rLum endocytosed by WT pMacs untreated or pretreated with chlorpromazine (CPZ) or filipin (FLP) dissolved in dimethylsulfoxide (DMSO), or DMSO vehicle control, stained with anti–His-FITC and F4/80-Pacific Blue, and rLum uptake analyzed by flow cytometry. The cumulative data shows percentage of rLum-ingested pMacs ($n = 7$ to 8 technical replicates from three independent experiments). (*B*) MFI of rLum in a representative flow cytometry histogram of rLum-ingested WT pMacs and cumulative data are from three independent experiments. (*C*) Colocalization of ingested rLum with Transferrin$^+$ or Cav1$^+$ vesicles in WT pMacs by confocal microscopy. A representative image of four to five fields from two independent experiments is shown. (*D*) Colocalization of ingested rLum (His-tag) with Rab5$^+$ early, Rab11$^+$ recycling, Rab7$^+$ late endosomes, and LAMP1$^+$ endolysosomes in WT pMacs by confocal microscopy. One of eight fields from two independent experiments shown. The histograms are cross-line scans of the fluorescence intensities of the merged panels. (*E*) WT pMacs untreated or LPS treated for 60 min and incubated with rLum (His-tag). The merged panels show colocalization of TLR4 and rLum and colocalization of rLum with FITC-LPS. The images are from one of seven fields from two independent experiments. The error bars represent mean ± SEM, two-tailed Student's *t* test (*A* and *B*). *$P < 0.05$ and ****$P < 0.0001$. (Scale bar in *C*, *D*, and *E*, 10 μm.)

in TLR9 signals. Bgn may also regulate TLR9 response, as $Bgn^{-/-}$ pMacs show greater induction of TNF-α after CpG DNA stimulation than heterozygous $Bgn^{+/-}$ pMacs (Fig. 8*D*).

TLR9 is synthesized in the endoplasmic reticulum (ER) and transported to an intermediate VAMP3$^+$ late endosome and to lysosome-related organelles (LRO), where its activated forms (51, 52) respond to pathogenic DNA and induce proinflammatory cytokines and type I interferons, respectively (40, 53). The human and mouse cytokine data suggest a suppressive role for Lum in TLR9 activities in VAMP3+ endosomes and LRO. We examined whether location of the TLR9 receptor is different in $Lum^{-/-}$ and WT pMacs after CpG DNA encounter. Cells treated with CpG DNA for 180 min were stained for TLR9 and VAMP3. By confocal microscopy, we found TLR9 and VAMP3 to show slightly higher colocalization in $Lum^{-/-}$ compared with WT pMacs (Fig. 8 *E* and *F*). Furthermore, as Lum colocalizes with Rabs, it may also interface with Rab-TLR9 regulations, although there is little change in the expression of *Rab* genes in LPS- or CpG DNA–stimulated pMacs (*SI Appendix*, Fig. S8*D*). We also wondered whether Lum regulates CpG DNA entry and trafficking into cells, and to that end, FITC-tagged CpG DNA uptake in $Lum^{-/-}$ pMacs is clearly elevated compared with WT pMacs (Fig. 8 *G* and *H*). By contrast, FITC-dextran uptake, indicative of general micropinocytosis, is comparable in $Lum^{-/-}$ and WT pMacs (*SI Appendix*, Fig. S8*E*). We further detected a strong vesicular colocalization between CpG DNA and rLum in WT pMacs (Fig. 8*I*), suggesting cotrafficking of Lum and CpG DNA within the cell. Given their strong colocalization, we asked whether Lum binds to CpG DNA; we detected a dose-dependent binding between Lum and CpG DNA in a solid-phase binding assay. rBgn shows avid binding as well, while rDcn shows little to no binding to CpG DNA (Fig. 8*J*). In a competitive binding assay, rLum competes with CD14 for CpG DNA binding in a dose-dependent manner (Fig. 8*K*). Finally, there is no colocalization between Lum and TLR9 in WT pMacs (*SI Appendix*, Fig. S8*F*). Overall, these results suggest that beyond having a small effect on trafficking of TLR9 itself, Lum is largely affecting the movement of its ligand. This implies that Lum is likely to bind microbial DNA to deter its entry into cells, and the DNA taken up in association with Lum is

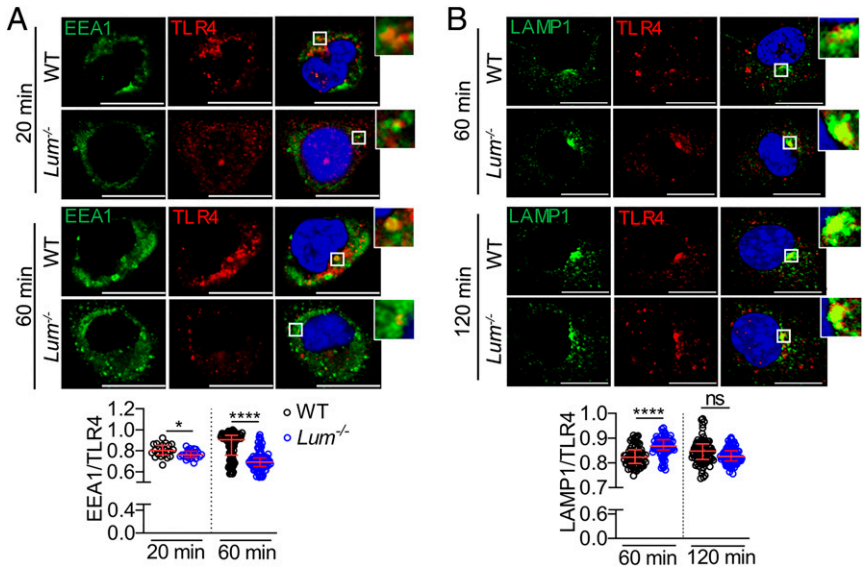

Fig. 7. Lumican delays TLR4 trafficking to endolysosomes in pMacs. (*A*) TLR4 localization in EEA1$^+$ early endosomes by confocal microscopy in WT and *Lum*$^{-/-}$ pMacs stimulated with LPS. Representative images from three independent experiments are shown. The cumulative Manders' Coefficient shows median and interquartile range of $n = 24$ cells/20 min and 93 to 99 cells/60 min from seven to nine fields from three independent experiments. (*B*) TLR4 localization in LAMP1$^+$ endolysosomes by confocal microscopy in LPS-stimulated WT and *Lum*$^{-/-}$ pMacs. The cumulative Manders' Coefficient shows median and interquartile range of $n = 66$ to 77 cells/60 min and 75 to 88 cells/120 min from 15 to 20 fields from three independent experiments. Significance was determined by a two-tailed Student's *t* test. *$P < 0.05$ and ****$P < 0.0001$. (Scale bar in *A* and *B*, 13 μm.)

preferentially delivered to TLR9-poor subcellular locations (Fig. 9). These in vitro and ex vivo data are also consistent with the negative correlation with anti-DNA antibody and levels of Lum in sepsis patients' plasma and increased autoantibodies in CIP-challenged *Lum*$^{-/-}$ mice.

Discussion

This study makes major advancements in understanding ECM functions in TLR mediated innate immunity and inflammatory responses. We identified a protective role for Lum via its TLR-regulatory functions in human and mouse sepsis. Lum released into the blood stream from a remodeling vascular ECM (54) or synthesized de novo by activated fibroblasts may play a dual role. First, by promoting TLR4 signals, Lum may help to restrict bacterial expansion; and second, by binding to DNA, it may simultaneously reduce the uptake of DNA and sequester any internalized DNA, either self or pathogen derived, to mitigate TLR9 signals, as shown in a schematic representation of Lum cross-talks with TLR4 and TLR9 signals (Fig. 9). Lum-mediated TLR9 signal suppression may help to restrict autoimmunity or antiviral inflammatory responses. In support, an earlier experimental autoimmune encephalomyelitis study reported *Lum*$^{-/-}$ mice to have worse disease; however, TLR9 signals were not investigated in that study (55). Bgn, a Lum-like SLRP, was found to be associated with overexpression and overactive TLR2 and TLR4 signals in autoimmune lupus nephritis, but TLR9 signals were not explored in that model either (56).

We uncovered a mechanism by which paracrine ECM Lum adheres to macrophages, is subsequently taken up by caveolar- and clathrin-mediated endocytosis, and regulates TLR signaling by controlling receptor and ligand trafficking. Unlike Bgn, Lum is not detectably expressed by basal or activated macrophages (20) but is expressed by injured epithelia (57), cytokine-activated fibroblasts (47), and as we show here, by fibroblasts of the visceral omentum, an important source of immunomodulatory ECM proteins, chemokines, and cytokines. The ECM has been envisioned as a facilitator of cell migration and maintaining critical concentrations of cytokines, growth factors, and pathogens. In some instances, specific ECM components have been cited as going rogue and stimulating cell surface TLRs by themselves as danger-associated molecular patterns (23). These studies were consistent with the idea that the role of the ECM ends at the cell surface. That ingested ECM proteins control vesicular trafficking of pathogen recognition receptors and ligands, as we show, is a paradigm shift in our understanding of ECMs in immune cell functions.

We have reported LPS hyporesponsiveness in *Lum*$^{-/-}$ mice (20), and all three SLRPs have been linked to inflammation, but their underlying mechanisms were obscure (58–60). During LPS recognition, CD14- and TLR4-containing supramolecular organizing centers form in cell surface lipid-rich microdomains (34–36) and subsequently in intracellular organelle membranes for signal propagation (29). Our current study suggests that Lum is drawn into these organizing centers with extensive functional consequences. Soluble Bgn and Dcn also promote TLR2 and 4 signals (9, 23), but their mechanism of action within cells are not understood. While Lum does not bind TLR4, its N-terminal tyrosine (Y20) binds CD14, and here we identify Cav1 as a lumican-binding partner in CD14-rich rafts. In fact, Lum's affinity for Cav1 (KA = 7.88×10^{11} M^{-1}; KD = 1.27×10^{-12} M) is much stronger than its affinity for CD14 (KA = 2.45×10^{6} M^{-1}; KD = 4.66×10^{-7} M) (21). Lum not only binds Cav1 but through its F228 epitope promotes Cav1 surface presentation. Interestingly, the Lum Y20 epitope is sufficient for maintaining surface CD14, but both Y20 and F228 sites are needed for surface presentation of TLR4 and the induction of TNF-α by LPS at the cell surface. Notably, by SPR, we found no Cav1-binding or surface-presentation functions in Bgn or Dcn. The Cav1 binding epitope in Lum resides in its LRR7 motif; Bgn and Dcn, only 32 and 30% similar at the amino acid level, lack the Cav1 binding site. The Lum LRR7 is also its major collagen-interacting region, and LRR motifs in SLRPs are typically used for collagen fibril association. Thus, in a homeostatic ECM, Lum–collagen interaction may limit its interactions with immune cells. Lum also binds to Fas (CD95) and *β*-2 integrin (61, 62), indicating that multiple interactions may be used to capture Lum at the immune

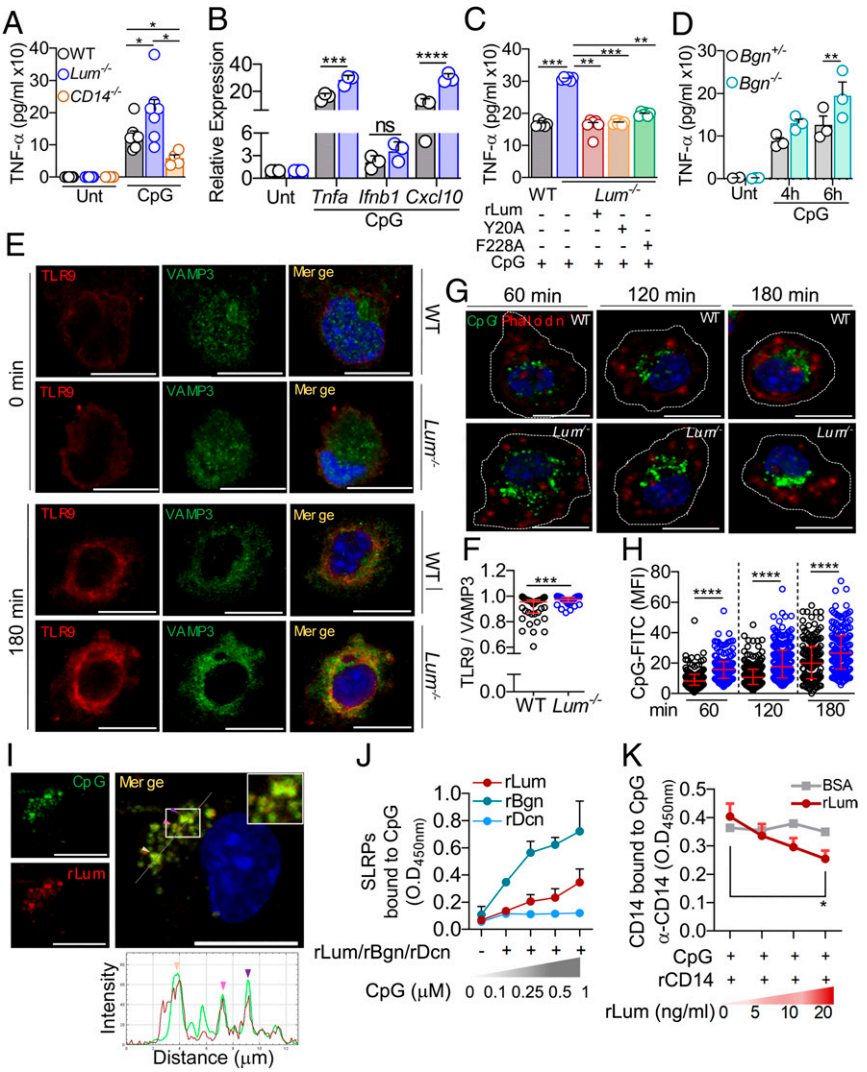

Fig. 8. Lumican suppresses TLR9 response in macrophages. (*A*) TNF-α (ELISA) in WT, *Lum*$^{-/-}$, and CD14$^{-/-}$ pMac cultures stimulated with CpG DNA for 6 h (n = 5 to 7 mice per genotype). (*B*) *Tnfa*, *Ifnb1*, and *Cxcl10* gene expression by qPCR in elicited pMacs, untreated (Unt), or CpG stimulated for 6 h (n = 3 mice/genotype). (*C*) WT and *Lum*$^{-/-}$ pMacs were pretreated with or without rLum, Y20A or F228A, and CpG for 6 h. TNF-α was measured in the media by ELISA (n = 6 technical replicates from three independent experiments). (*D*) TNF-α (ELISA) in the media of *Bgn*$^{+/-}$ and *Bgn*$^{-/-}$ pMacs stimulated with CpG (n = 3 mice from three independent experiments). (*E*) A representative image of TLR9 and VAMP3^{+} endosome colocalization by confocal microscopy in WT and *Lum*$^{-/-}$ pMacs at 0 and 180 min after CpG DNA treatment. (*F*) Cumulative data (n = 40 to 43 cells) from (*E*) showing Manders' coefficient of colocalization, median, and interquartile range from three independent experiments. (*G*) A representative confocal microscopy of CpG-FITC uptake by WT and *Lum*$^{-/-}$ pMacs incubated with 1 μM CpG-FITC, Phalloidin counterstained. (*H*) Cumulative data for (*G*) showing median with interquartile range of CpG-FITC in 114 to 222 cells from three independent experiments. (*I*) rLum and CpG-FITC colocalization. CpG-FITC and His-tag-rLum (10 μg/mL)–treated WT pMacs stained with anti–His-AF 555. A representative image from two independent experiments. The histogram depicts cross-line scans of fluorescence intensities of the boxed area. (*J*) rLum/rBgn/rDcn bound to CpG DNA-biotin in solid-phase binding assays. (*K*) Binding of rCD14 to CpG-biotin in the presence of increasing soluble rLum or bovine serum albumin (BSA). n = 3 independent experiments (*J* and *K*). The error bars represent SEM, two-tailed Student's t test (*A–D*, *F*, *H*, and *K*). *P < 0.05, **P < 0.01, ***P < 0.001, ****P < 0.0001. (Scale bar in *E*, *G*, and *I*, 10 μm.)

cell surface. Interactions of Bgn and Dcn with collagen fibrils may similarly limit their cross-talk with growth factors and immune cell receptors that remain to be defined.

Our results demonstrate that Lum increases TLR4 levels at the cell surface and in LPS^{+} endosomes, while it delays lysosomal degradation of TLR4 for enhancement of proinflammatory and protective type I interferon signals. It is known that endocytosis of LPS-stimulated TLR4 leads to its lysosomal turnover and signal attenuation as well as CD14-aided recognition of endosomal LPS and MyD88-independent induction of type I interferon. Our findings implicate additional regulations by Lum at these endosomal sites where it colocalizes with early, late, and recycling endosomal Rab GTPases (63). Further studies are needed to determine whether specific interactions of Lum with Rabs or other TLR adaptors are involved.

In contrast to its effects on TLR4, Lum exerts a strong negative regulation on TLR9 signals. We discovered that Bgn also reduces TLR9 signals, but its exact mode of regulation is not understood yet. TLR9 is exquisitely regulated by multiple proteins, such as ER resident UNC93B1 and other adaptor proteins forms (51, 52). Here, ECM-derived Lum may exert an extra layer of control that was hitherto unrecognized. In addition to influencing intracellular trafficking of TLR9, intriguingly, Lum may have a larger role in sequestering DNA ligands in early endosomes that are TLR9 poor

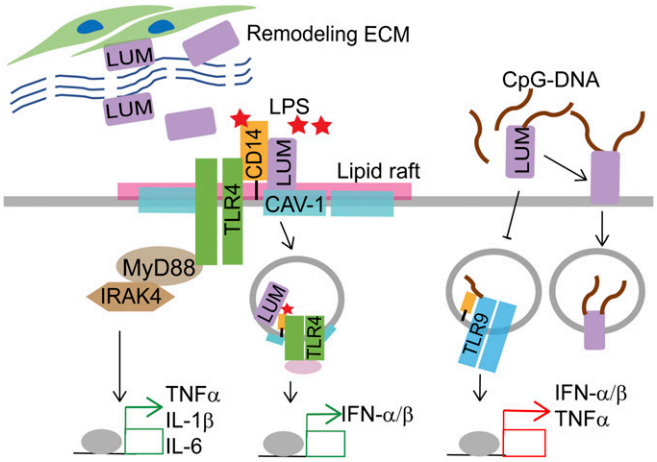

Fig. 9. Regulations of TLR4 and TLR9 signals in macrophages by Lumican. Synthesized de novo by activated fibroblasts or released in the tissue microenvironment from a remodeling ECM, lumican enhances TLR4 and restricts TLR9 signals in macrophages.

and thereby dampen the TLR9 response. In a polymicrobial sepsis challenge, the *Lum*$^{-/-}$ mice show early impairments in inflammatory signaling and infection control, while anti-DNA antibodies and autoimmune responses increase, possibly a consequence of muted TLR4 and aggravated TLR9 responses.

Our findings identify previously unidentified mechanisms employed by the ECM to modulate immune cell functions with far-reaching implications. First, lipid raft microdomains are important to many signaling platforms that may be profoundly influenced by ECM proteins. These ECM–lipid raft interactions may also be relevant to viral entry and drug-delivery mechanisms, which should be investigated in the future. Second, macrophages and DCs ingest Lum from their vicinal ECM; this may be an important way that antigen-presenting cells are instructed in their local tissue-specific ECM niche. Locally ingested ECM proteins may thus have a significant and as yet unexplored influence on macrophage heterogeneity, their transcriptional programming in tissue regeneration, and fibrosis (64). In fact, the reported transcriptomic programming of tissue resident macrophages that reduce TLR9 responsiveness to apoptotic cell nucleic acids and inflammatory signals from the local microenvironment (65) may include engulfed ECM cargo, like Lum. An intriguing consideration is that in immune-privileged barrier tissues like the cornea, Lum may be poised to promote TLR4-innate immunity to curb expansion of commensal and pathogenic bacteria, while limiting TLR9-mediated inflammatory response to microbial and apoptotic cell DNA to assure corneal clarity. Our earlier finding that Lum promotes Fas-FasL–mediated apoptosis further supports its role in restricting T cell–mediated adaptive immunity in the cornea. Our discovery that both Lum and Bgn bind DNA and dampen TLR9 signals underscores the need to re-evaluate mechanisms by which ECM SLRPs regulate inflammatory and autoimmune-provoking signals. Regulation of TLR and ligand trafficking by endocytosed ECM proteins may be a mechanism by which the ECM exerts a localized influence on immune responses.

Materials and Methods

Human Subjects and Sample Collection. Recruitment of all subjects were approved by the Institutional Review Board at New York University Langone Health, and written informed consents were provided by subjects before participation in this study. Healthy individuals were all adults and with no reported disease or infection. Sepsis patients were adults with positive blood cultures on or just before the day of sample collection. Methods for venous blood collection and PBMC and plasma samples are described in *SI Appendix*.

Mice. All protocols were approved by the New York University Institutional Animal Care and Use Committee. All mouse strains were in the C57BL/6J background. Breeding pairs of C57BL/6J (Stock No. 000664), *CD14*$^{-/-}$ (Stock No. 003726), and *Cav1*$^{-/-}$ (Stock No. 007083) mice, from the Jackson Laboratories, *Bgn*$^{-/-}$, *Bgn*$^{-/0}$ (11, 13), *Lum*$^{+/-}$, and *Lum*$^{-/-}$ (in house) (12) were maintained in a specific pathogen-free mouse facility at New York University, School of Medicine with 12-h light/dark cycle and ad libitum feeding. We used 8- to 16-wk-old mice for all experiments, with equal numbers of animals of both sexes within each experiment.

Statistical Analysis. All the experiments were repeated two to four times as indicated. Comparisons between multiple groups were performed by one-way or two-way ANOVA followed by multiple comparisons analysis. Correlation analysis were performed using Pearson, and comparisons between two groups by two-tailed nonparametric Student's *t* test using Graph Pad Prism version 8.

Extended Methods. Procedures for all cell culture assays, mouse polymicrobial sepsis, flow cytometry, qRT-PCR, enzyme-linked immunosorbent assay (ELISA), and biochemical assays are described in *SI Appendix, Supplementary Methods*.

All materials used in this study are listed in *SI Appendix*, Table S1.

Data Availability. Bulk RNA sequencing data have been deposited in the National Center for Biotechnology Information GEO database (accession no. GSE174026). All other study data are included in the article and/or supporting information.

ACKNOWLEDGMENTS. We thank Drs. Abdel R. A. Hamad, Dave Serreze, and Reza Dana for insightful discussions, Indira Chakravarti for editing the manuscript, and Nan Hu for assistance in RNA sequence analysis. This work was supported by NIH Grant No. EY11654 and Grant No. EY030917 to S.C. and Grant No. 1UM1AI148574 to M.J.M.

1. R. O. Hynes, A. Naba, Overview of the matrisome--an inventory of extracellular matrix constituents and functions. *Cold Spring Harb. Perspect. Biol.* **4**, a004903 (2012).
2. M. K. Gordon, R. A. Hahn, Collagens. *Cell Tissue Res.* **339**, 247–257 (2010).
3. Y. Zhou *et al.*, Extracellular matrix in lung development, homeostasis and disease. *Matrix Biol.* **73**, 77–104 (2018).
4. S. Ricard-Blum, R. Salza, Matricryptins and matrikines: Biologically active fragments of the extracellular matrix. *Exp. Dermatol.* **23**, 457–463 (2014).
5. K. E. Rudd *et al.*, Global, regional, and national sepsis incidence and mortality, 1990-2017: Analysis for the global burden of disease study. *Lancet* **395**, 200–211 (2020).
6. S. Chakravarti, R. L. Stallings, N. SundarRaj, P. K. Cornuet, J. R. Hassell, Primary structure of human lumican (keratan sulfate proteoglycan) and localization of the gene (LUM) to chromosome 12q21.3-q22. *Genomics* **27**, 481–488 (1995).
7. A. C. Ng *et al.*, Human leucine-rich repeat proteins: A genome-wide bioinformatic categorization and functional analysis in innate immunity. *Proc. Natl. Acad. Sci. U.S.A.* **108** (suppl. 1), 4631–4638 (2011).
8. P. A. McEwan, P. G. Scott, P. N. Bishop, J. Bella, Structural correlations in the family of small leucine-rich repeat proteins and proteoglycans. *J. Struct. Biol.* **155**, 294–305 (2006).
9. R. Merline, R. M. Schaefer, L. Schaefer, The matricellular functions of small leucine-rich proteoglycans (SLRPs). *J. Cell Commun. Signal.* **3**, 323–335 (2009).
10. J. Frikeche, G. Maiti, S. Chakravarti, Small leucine-rich repeat proteoglycans in corneal inflammation and wound healing. *Exp. Eye Res.* **151**, 142–149 (2016).
11. S. Chen, D. E. Birk, The regulatory roles of small leucine-rich proteoglycans in extracellular matrix assembly. *FEBS J.* **280**, 2120–2137 (2013).
12. S. Chakravarti *et al.*, Lumican regulates collagen fibril assembly: Skin fragility and corneal opacity in the absence of lumican. *J. Cell Biol.* **141**, 1277–1286 (1998).
13. T. Xu *et al.*, Targeted disruption of the biglycan gene leads to an osteoporosis-like phenotype in mice. *Nat. Genet.* **20**, 78–82 (1998).
14. K. G. Danielson *et al.*, Targeted disruption of decorin leads to abnormal collagen fibril morphology and skin fragility. *J. Cell Biol.* **136**, 729–743 (1997).
15. A. E. Mellgren *et al.*, Development of congenital stromal corneal dystrophy is dependent on export and extracellular deposition of truncated decorin. *Invest. Ophthalmol. Vis. Sci.* **56**, 2909–2915 (2015).
16. F. Wu, S. Chakravarti, Differential expression of inflammatory and fibrogenic genes and their regulation by NF-kappaB inhibition in a mouse model of chronic colitis. *J. Immunol.* **179**, 6988–7000 (2007).
17. K. Lohr *et al.*, Extracellular matrix protein lumican regulates inflammation in a mouse model of colitis. *Inflamm. Bowel Dis.* **18**, 143–151 (2012).
18. A. Hultgårdh-Nilsson, J. Borén, S. Chakravarti, The small leucine-rich repeat proteoglycans in tissue repair and atherosclerosis. *J. Intern. Med.* **278**, 447–461 (2015).

19. L. T. Hsieh, M. V. Nastase, J. Zeng-Brouwers, R. V. Iozzo, L. Schaefer, Soluble biglycan as a biomarker of inflammatory renal diseases. *Int. J. Biochem. Cell Biol.* **54**, 223–235 (2014).
20. F. Wu *et al*., A novel role of the lumican core protein in bacterial lipopolysaccharide-induced innate immune response. *J. Biol. Chem.* **282**, 26409–26417 (2007).
21. H. Shao *et al*., Extracellular matrix lumican promotes bacterial phagocytosis, and Lum-/- mice show increased *Pseudomonas aeruginosa* lung infection severity. *J. Biol. Chem.* **287**, 35860–35872 (2012).
22. H. Shao, S. G. Scott, C. Nakata, A. R. Hamad, S. Chakravarti, Extracellular matrix protein lumican promotes clearance and resolution of *Pseudomonas aeruginosa* keratitis in a mouse model. *PLoS One* **8**, e54765 (2013).
23. L. Schaefer *et al*., The matrix component biglycan is proinflammatory and signals through Toll-like receptors 4 and 2 in macrophages. *J. Clin. Invest.* **115**, 2223–2233 (2005).
24. R. Merline *et al*., Signaling by the matrix proteoglycan decorin controls inflammation and cancer through PDCD4 and microRNA-21. *Sci. Signal.* **4**, ra75 (2011).
25. J. P. Orgel, A. Eid, O. Antipova, J. Bella, J. E. Scott, Decorin core protein (decoron) shape complements collagen fibril surface structure and mediates its binding. *PLoS One* **4**, e7028 (2009).
26. S. Kalamajski, Å. Oldberg, Homologous sequence in lumican and fibromodulin leucine-rich repeat 5-7 competes for collagen binding. *J. Biol. Chem.* **284**, 534–539 (2009).
27. J. Melrose *et al*., Fragmentation of decorin, biglycan, lumican and keratocan is elevated in degenerate human meniscus, knee and hip articular cartilages compared with age-matched macroscopically normal and control tissues. *Arthritis Res. Ther.* **10**, R79 (2008).
28. T. Kawai, S. Akira, The role of pattern-recognition receptors in innate immunity: Update on Toll-like receptors. *Nat. Immunol.* **11**, 373–384 (2010).
29. K. A. Fitzgerald, J. C. Kagan, Toll-like receptors and the control of immunity. *Cell* **180**, 1044–1066 (2020).
30. B. Park *et al*., Proteolytic cleavage in an endolysosomal compartment is required for activation of Toll-like receptor 9. *Nat. Immunol.* **9**, 1407–1414 (2008).
31. S. E. Ewald, G. M. Barton, Nucleic acid sensing Toll-like receptors in autoimmunity. *Curr. Opin. Immunol.* **23**, 3–9 (2011).
32. A. Haziot *et al*., The monocyte differentiation antigen, CD14, is anchored to the cell membrane by a phosphatidylinositol linkage. *J. Immunol.* **141**, 547–552 (1988).
33. S. D. Wright, R. A. Ramos, P. S. Tobias, R. J. Ulevitch, J. C. Mathison, CD14, a receptor for complexes of lipopolysaccharide (LPS) and LPS binding protein. *Science* **249**, 1431–1433 (1990).
34. Y. Nagai *et al*., Essential role of MD-2 in LPS responsiveness and TLR4 distribution. *Nat. Immunol.* **3**, 667–672 (2002).
35. M. Triantafilou *et al*., Combinational clustering of receptors following stimulation by bacterial products determines lipopolysaccharide responses. *Biochem. J.* **381**, 527–536 (2004).
36. B. S. Park *et al*., The structural basis of lipopolysaccharide recognition by the TLR4-MD-2 complex. *Nature* **458**, 1191–1195 (2009).
37. T. Shuto *et al*., Membrane-anchored CD14 is required for LPS-induced TLR4 endocytosis in TLR4/MD-2/CD14 overexpressing CHO cells. *Biochem. Biophys. Res. Commun.* **338**, 1402–1409 (2005).
38. I. Zanoni *et al*., CD14 controls the LPS-induced endocytosis of Toll-like receptor 4. *Cell* **147**, 868–880 (2011).
39. Z. Jiang *et al*., CD14 is required for MyD88-independent LPS signaling. *Nat. Immunol.* **6**, 565–570 (2005).
40. E. Latz *et al*., TLR9 signals after translocating from the ER to CpG DNA in the lysosome. *Nat. Immunol.* **5**, 190–198 (2004).
41. C. L. Baumann *et al*., CD14 is a coreceptor of Toll-like receptors 7 and 9. *J. Exp. Med.* **207**, 2689–2701 (2010).
42. R. G. Parton, K. Simons, The multiple faces of caveolae. *Nat. Rev. Mol. Cell Biol.* **8**, 185–194 (2007).
43. T. H. Tsai *et al*., Impaired Cd14 and Cd36 expression, bacterial clearance, and Toll-like receptor 4-Myd88 signaling in caveolin-1-deleted macrophages and mice. *Shock* **35**, 92–99 (2011).
44. M. E. Starr *et al*., A new cecal slurry preparation protocol with improved long-term reproducibility for animal models of sepsis. *PLoS One* **9**, e115705 (2014).
45. J. Rivera-Correa *et al*., Plasmodium DNA-mediated TLR9 activation of T-bet^{+} B cells contributes to autoimmune anaemia during malaria. *Nat. Commun.* **8**, 1282 (2017).
46. T. Berlin *et al*., Autoantibodies in nonautoimmune individuals during infections. *Ann. N. Y. Acad. Sci.* **1108**, 584–593 (2007).
47. D. Pilling, V. Vakil, N. Cox, R. H. Gomer, TNF-α-stimulated fibroblasts secrete lumican to promote fibrocyte differentiation. *Proc. Natl. Acad. Sci. U.S.A.* **112**, 11929–11934 (2015).
48. L. H. Jackson-Jones *et al*., Stromal cells covering omental fat-associated lymphoid clusters trigger formation of neutrophil aggregates to capture peritoneal contaminants. *Immunity* **52**, 700–715.e6 (2020).
49. Y. Tan, I. Zanoni, T. W. Cullen, A. L. Goodman, J. C. Kagan, Mechanisms of Toll-like receptor 4 endocytosis reveal a common immune-evasion strategy used by pathogenic and commensal bacteria. *Immunity* **43**, 909–922 (2015).
50. J. Couet, S. Li, T. Okamoto, T. Ikezu, M. P. Lisanti, Identification of peptide and protein ligands for the caveolin-scaffolding domain. Implications for the interaction of caveolin with caveolae-associated proteins. *J. Biol. Chem.* **272**, 6525–6533 (1997).
51. K. Takahashi *et al*., A protein associated with Toll-like receptor (TLR) 4 (PRAT4A) is required for TLR-dependent immune responses. *J. Exp. Med.* **204**, 2963–2976 (2007).
52. K. Tabeta *et al*., The Unc93b1 mutation 3d disrupts exogenous antigen presentation and signaling via Toll-like receptors 3, 7 and 9. *Nat. Immunol.* **7**, 156–164 (2006).
53. M. Sasai, M. M. Linehan, A. Iwasaki, Bifurcation of Toll-like receptor 9 signaling by adaptor protein 3. *Science* **329**, 1530–1534 (2010).
54. J. L. Funderburgh, M. L. Funderburgh, M. M. Mann, G. W. Conrad, Arterial lumican. Properties of a corneal-type keratan sulfate proteoglycan from bovine aorta. *J. Biol. Chem.* **266**, 24773–24777 (1991).
55. E. F. Castillo *et al*., Lumican negatively controls the pathogenicity of murine encephalitic TH17 cells. *Eur. J. Immunol.* **46**, 2852–2861 (2016).
56. K. Moreth *et al*., The proteoglycan biglycan regulates expression of the B cell chemoattractant CXCL13 and aggravates murine lupus nephritis. *J. Clin. Invest.* **120**, 4251–4272 (2010).
57. S. Saika *et al*., Role of lumican in the corneal epithelium during wound healing. *J. Biol. Chem.* **275**, 2607–2612 (2000).
58. M. V. Nastase, R. V. Iozzo, L. Schaefer, Key roles for the small leucine-rich proteoglycans in renal and pulmonary pathophysiology. *Biochim. Biophys. Acta* **1840**, 2460–2470 (2014).
59. H. Frey, N. Schroeder, T. Manon-Jensen, R. V. Iozzo, L. Schaefer, Biological interplay between proteoglycans and their innate immune receptors in inflammation. *FEBS J.* **280**, 2165–2179 (2013).
60. C. W. Frevert, J. Felgenhauer, M. Wygrecka, M. V. Nastase, L. Schaefer, Danger-associated molecular patterns derived from the extracellular matrix provide temporal control of innate immunity. *J. Histochem. Cytochem.* **66**, 213–227 (2018).
61. N. Vij, L. Roberts, S. Joyce, S. Chakravarti, Lumican regulates corneal inflammatory responses by modulating Fas-Fas ligand signaling. *Invest. Ophthalmol. Vis. Sci.* **46**, 88–95 (2005).
62. S. Lee, K. Bowrin, A. R. Hamad, S. Chakravarti, Extracellular matrix lumican deposited on the surface of neutrophils promotes migration by binding to beta2 integrin. *J. Biol. Chem.* **284**, 23662–23669 (2009).
63. L. Langemeyer, F. Fröhlich, C. Ungermann, Rab GTPase function in endosome and lysosome biogenesis. *Trends Cell Biol.* **28**, 957–970 (2018).
64. T. A. Wynn, K. M. Vannella, Macrophages in tissue repair, regeneration, and fibrosis. *Immunity* **44**, 450–462 (2016).
65. A. W. Roberts *et al*., Tissue-resident macrophages are locally programmed for silent clearance of apoptotic cells. *Immunity* **47**, 913–927.e6 (2017).